AGU PUBLICATIONS

JGR

Journal of Geophysical Research: Solid Earth

RESEARCH ARTICLE
10.1002/2017JB014241

Key Points:
- Magnetic properties of variably serpentinized peridotites from the Dongbo ophiolite (SW Tibet) are investigated
- Magnetic susceptibility and magnetite abundance show peaks at approximately 25% of the degree of serpentinization
- Peridotites in 20-30% and >60% of serpentinization are major sources of magnetic anomalies in suture zones

Correspondence to:
Z. Li,
zhiyonli@outlook.com

Citation:
Li, Z., J. Zheng, B. M. Moskowitz, Q. Liu, Q. Xiong, J. Yang, and X. Hu (2017), Magnetic properties of serpentinized peridotites from the Dongbo ophiolite, SW Tibet: Implications for suture-zone magnetic anomalies, *J. Geophys. Res. Solid Earth*, *122*, 4814–4830, doi:10.1002/2017JB014241.

Received 24 MAR 2017
Accepted 27 JUN 2017
Accepted article online 29 JUN 2017
Published online 26 JUL 2017

Magnetic properties of serpentinized peridotites from the Dongbo ophiolite, SW Tibet: Implications for suture-zone magnetic anomalies

Zhiyong Li[1], Jianping Zheng[2], B. M. Moskowitz[3], Qingsheng Liu[1], Qing Xiong[4], Jingsui Yang[5], and Xiangyun Hu[1]

[1]Hubei Subsurface Multi-scale Imaging Key Laboratory, Institute of Geophysics and Geomatics, China University of Geosciences, Wuhan, China, [2]State Key Laboratory of Geological Processes and Mineral Resources, China University of Geosciences, Wuhan, China, [3]Institute for Rock Magnetism, Department of Earth Sciences, University of Minnesota, Twin Cities, Minneapolis, Minnesota, USA, [4]ARC Centre of Excellence for Core to Crust Fluid Systems and GEMOC, Department of Earth and Planetary Sciences, Macquarie University, Sydney, New South Wales, Australia, [5]Institute of Geology, Chinese Academy of Geological Sciences, Beijing, China

Abstract Magnetic properties of a suite of variably serpentinized peridotites from the Dongbo ophiolite, SW Tibet (China), have been investigated to determine the magnetic signatures of suture zones. The degree of serpentinization (S) for these peridotites is mainly in the range of $S < 60\%$. Petrography, mineral chemistry, and thermomagnetic analyses reveal that magnetite occurring in the interior of various serpentine veins is the predominant magnetic phase. Magnetic hysteresis and first-order reversal curve diagrams suggest that the magnetite is mixture of interacting single-domain, and pseudo-single-domain and/or multidomain particles. Superparamagnetic magnetite occurs in the S = 40–60% serpentinized but weakly magnetic dunites. Overall, the magnetite content and magnetic susceptibility increase consistently from ~0 to 20% of serpentinization and then decrease from S = 30 to 60%. Peak magnetite abundance is at S~25% (density, ~3.1 ± 0.05 g cm^{-3}) and may suggest localized enrichment of fluids. The low magnetite abundance in dunite results from low-temperature serpentinization. Finally, strong intensities of magnetization (1–10 Am^{-1}) reside in the $S > 60\%$ and S = 20–30% serpentinized peridotites, indicating that peridotites with such degrees of serpentinization contribute to the aeromagnetic anomalies within the Yarlung-Zangbo suture zone in south Tibet.

1. Introduction

Though some mantle xenoliths contain minor amounts of magnetite [e.g., *Ferré et al.*, 2013, 2014], most are mainly weakly magnetic [e.g., *Li et al.*, 2015; *Wasilewski and Mayhew*, 1992]. In contrast, serpentinized peridotites have attracted more attention because of both low density and high magnetization intensity and therefore are widely considered as a significant source for deep-seated lithospheric gravity, seismic velocity, and magnetic anomalies within oceanic ridge and subduction zone environments [e.g., *Blakely et al.*, 2005; *Bostock et al.*, 2002; *Q. S. Liu et al.*, 2015].

During the serpentinization of ultramafic rocks, silicates (e.g., olivine and pyroxene) release iron under the effects of fluid infiltration and produce magnetite, which strongly increases the magnetization intensity in shallow lithospheric systems [*Bina and Henry*, 1990; *Oufi et al.*, 2002]. The serpentinization process of peridotites generally involves multistage fluid-mineral reactions, and the production rate of magnetite is not linearly related to the degree of serpentinization [*Bach et al.*, 2006; *Toft et al.*, 1990]. Nearly complete yet magnetite-poor serpentinization indicates that the formation of magnetite could be decoupled from the direct hydration of olivine or pyroxene [*Evans et al.*, 2009; *Lafay et al.*, 2012]. Many studies have revealed that the formation and stability of serpentinization products (e.g., serpentine, brucite, and magnetite) involve multiple factors, such as silica activity, fluid/rock ratios, and temperature in the serpentinization process [e.g., *Frost and Beard*, 2007; *Klein et al.*, 2009, 2014].

The relationship between magnetic properties and the serpentinization process of peridotites is still under debate, and previous studies have mostly focused on abyssal peridotites [e.g., *Kelemen et al.*, 2004; *Oufi et al.*, 2002]. Equally important but not as well studied are magnetic properties of peridotites exposed in other tectonic settings, such as ultrahigh-pressure orogenic belts [*Liu et al.*, 2010] and suture zones

[*Bonnemains et al.*, 2016; *Maffione et al.*, 2014]. Here we present the magnetic properties combined with petrography and mineral chemistry of a suite of variably serpentinized peridotites from the Dongbo ophiolite located within the western part of the Yarlung-Zangbo suture zone in south Tibet (China). The study shows the magnetic variations of these peridotites at different stages of serpentinization and discusses the implications for suture-zone magnetic anomalies.

2. Geological Setting

Several suture zones are well defined separating the terranes from north to south in the Tibetan Plateau [e.g., *DeCelles et al.*, 2002; *Yin and Harrison*, 2000]. The Yarlung-Zangbo suture zone in the southernmost area marks the collision between the Lhasa block and the Indian plate, and numerous ophiolitic massifs crop out within this over 2000 km suture zone (Figure 1a). Dongbo, Pulan, and Dangqiong are the largest massifs in the western part of the Yarlung-Zangbo suture zone. The Dongbo peridotite massif covers an area of ~400 km^2 identified by aeromagnetic data [*Jiang et al.*, 2015; *Yang et al.*, 2011], but about one third of this massif is covered by Neogene-Quaternary sediments (Figure 1b). The peridotite massif is in fault contact with surrounding Late Triassic to Late Cretaceous mélanges, consisting of carbonates, clastic rocks, basic lavas, and cherts [*F. Liu et al.*, 2015]. Gabbro and pyroxenite dykes that intruded the peridotites yield crystallization ages of ~130–128 Ma (U-Pb dating on zircons) [*Xiong et al.*, 2011]. This intrusion of mafic dykes is consistent with widespread mafic magmatism at ~130–120 Ma within the whole Yarlung-Zangbo suture zone [e.g., *Wu et al.*, 2014; *Xiong et al.*, 2016].

The Dongbo peridotite massif is composed mainly of harzburgite, with minor lenses of dunite, lherzolite, and chromitite. Geochemical studies of rare earth elements and Re-Os isotopic compositions suggest that the peridotites were derived from heterogeneous Neo-Tethyan lithospheric mantle and experienced basaltic magma extraction in a spreading midocean-ridge setting and subsequent modification by percolating melts in a suprasubduction zone environment [*Niu et al.*, 2015]. The presence of ultrahigh-pressure, highly reduced and crustal-derived minerals in the Dongbo peridotites also suggests a complex recycling process in the mantle [*Xu et al.*, 2015].

3. Methods

3.1. Magnetic Measurements

Fresh specimens were prepared by sawing off weathered skins for magnetic measurements and thin sections. Density (ρ) and susceptibility (κ) were measured using a Sartorius balance (BT 423S) with a density determination kit and a Kappabridge susceptibility meter (KLY−3s), respectively, at the China University of Geosciences (CUG, Wuhan). Natural remanent magnetization (NRM) was measured using a JR-6A dual speed spinner magnetometer at the China Earthquake Administration (Beijing). Additional magnetic characterization experiments (hysteresis loops, AC susceptibility, high-temperature susceptibility, and low-temperature remanence) were carried out at the Institute for Rock Magnetism (IRM) in the University of Minnesota (Minneapolis-Saint Paul, USA).

Magnetic hysteresis loops, backfield remanence curves, and first-order reversal curves (FORCs) were measured at room temperature using a Princeton Measurements Corporation vibrating sample magnetometer (VSM Model 3900). The applied saturation field was 1.0 T. A total of 104 FORC curves per sample were measured, and FORCs were processed using FORCinel 3.0 [*Harrison and Feinberg*, 2008]. Hysteresis parameters (M_s, saturation magnetization; M_{rs}, saturation remanence; and B_c, coercivity) were calculated after paramagnetic slope correction over the interval of 0.7–1.0 T using the nonlinear approach-to-saturation fitting method by *Jackson and Solheid* [2010]. Coercivity of remanence (B_{cr}) was determined from DC backfield remanence curves.

Crushed powders (less than 60 mesh, ~250 μm) were prepared for thermomagnetic analyses. High-temperature susceptibility experiments were conducted on a Kappabridge (MFK1-FA) from room temperature to ~700°C in an argon environment. Low-temperature demagnetization (LTD) experiments were performed using a Quantum Design Magnetic Properties Measurement System superconducting susceptometer (MPMS) from 20 K to 300 K, following the *FC-ZFC-LTSIRM-RTSIRM LTD* measurement sequence (refer to *Bilardello and Jackson* [2013]). Samples were first cooled from room temperature to 20 K in 2.5 T field

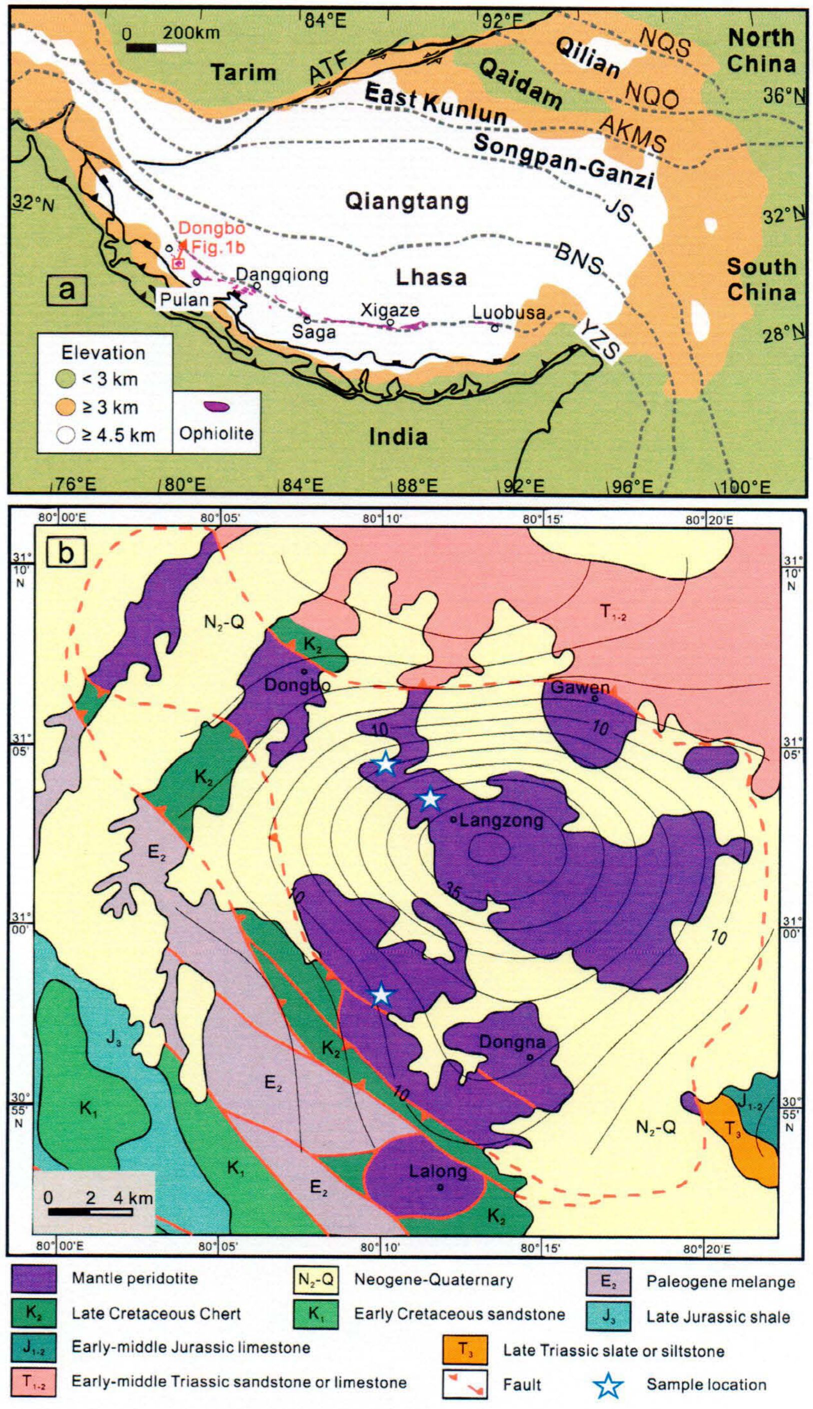

Figure 1. (a) Simplified tectonic map of the Tibetan Plateau (modified after *DeCelles et al.* [2002]) and ophiolites cropping out along the Yarlung-Zangbo suture zone (modified after *Dai et al.* [2011]). (b) Geological sketch map of the Dongbo ophiolite (modified after *Yang et al.* [2011]) with regional aeromagnetic anomalies. Isomagnetic contours (5 nT interval) are based on aeromagnetic anomaly data after reduction to pole and 5 km upward continuation [*Jiang et al.*, 2016]. Abbreviations: YZS, Yarlung-Zangbo suture; BNS, Bangong-Nujiang suture; JS, Jinsha suture; AKMS, Anyimaqen-Kunlun-Muztagh suture; NQO, North Qaidam orogen; NQS, North Qilian suture; ATF, Altyn Tagh Fault.

Table 1. Density and Magnetic Parameters of the Dongbo Peridotites From SW Tibet[a]

Sample	Lithology	ρ g cm^{-3}	κ 10^{-6} (SI)	χ 10^{-8} m^3 kg^{-1}	J_i Am^{-1}	NRM Am^{-1}	Q_n	M_s 10^{-3} Am^2 kg^{-1}	M_{rs} 10^{-3} Am^2 kg^{-1}	B_c mT	B_{cr} mT	B_{cr}/B_c	M_{rs}/M_s	M_{rs}/χ 10^3 Am^{-1}	χ_{para} 10^{-8} m^3 kg^{-1}	m (%)	S (%)
DB11-12	Dunite	2.888	767	26.5	0.03	0.09	2.9	15.2	1.98	14.8	34.8	2.35	0.13	7.48	7.4	0.02	52.5
DB11-57	Dunite	2.879	477	16.6	0.02	0.10	5.5	3.36	0.54	18.4	43.5	2.37	0.16	3.28	9.7	0.00	53.7
DB11-58	Dunite	2.897	549	19.0	0.02	1.26	58.7	9.21	1.97	22.8	48.6	2.14	0.21	10.4	13.3	0.01	51.3
DB11-59	Dunite	2.944	637	21.6	0.02	0.33	13.4	11.5	1.88	20.6	59.4	2.88	0.16	8.67	13.5	0.01	45.3
DB11-60	Dunite	2.974	660	22.2	0.03	1.89	73.4	14.1	3.70	26.5	51.9	1.96	0.26	16.7	10.8	0.02	41.5
DB11-08	Harzburgite	3.176	1,046	32.9	0.04	0.01	0.2	42.5	8.84	17.2	27.8	1.61	0.21	26.8	16.5	0.05	15.7
DB11-09	Harzburgite	3.278	1,550	47.3	0.06	0.02	0.3	51.3	9.15	13.0	22.4	1.73	0.18	19.3	14.2	0.06	2.8
DB11-11	Harzburgite	3.275	931	28.4	0.04	0.02	0.4	11.5	2.88	28.8	58.1	2.02	0.25	10.1	12.2	0.01	3.2
DB11-13	Harzburgite	3.317	863	26.0	0.03	0.01	0.3	14.8	4.19	22.5	39.0	1.73	0.28	16.1	14.5	0.02	0.0
DB11-14	Harzburgite	3.265	1,433	43.9	0.06	0.01	0.3	48.7	13.3	26.5	49.5	1.87	0.27	30.2	15.1	0.05	4.4
DB11-15	Harzburgite	3.026	997	33.0	0.04	0.01	0.2	49.9	10.1	24.7	48.5	1.97	0.20	30.7	14.0	0.05	34.9
DB11-16	Harzburgite	3.288	777	23.6	0.03	0.00	0.1	11.5	3.57	22.7	43.8	1.93	0.31	15.1	14.0	0.01	1.6
DB11-17	Harzburgite	2.966	1,066	35.9	0.04	0.01	0.3	28.4	4.76	14.8	29.1	1.97	0.17	13.2	12.7	0.03	42.6
DB11-18	Harzburgite	3.290	1,310	39.8	0.05	0.01	0.3	36.9	7.19	18.6	34.6	1.86	0.19	18.0	14.0	0.04	1.2
DB11-19	Harzburgite	3.267	1,036	31.7	0.04	0.02	0.5	24.7	6.92	24.9	43.0	1.72	0.28	21.8	14.2	0.03	4.2
DB11-20	Harzburgite	3.219	993	30.9	0.04	0.01	0.3	47.7	11.7	22.6	36.7	1.63	0.25	38.1	15.3	0.05	10.3
DB11-32	Harzburgite	3.135	1,444	46.1	0.06	0.02	0.4	67.2	12.5	15.1	26.8	1.78	0.19	27.1	13.8	0.07	21.0
DB11-33	Harzburgite	3.085	2,699	87.5	0.11	0.04	0.4	58.8	11.8	16.0	28.4	1.77	0.20	13.5	14.6	0.06	27.4
DB11-34	Harzburgite	3.173	1,133	35.7	0.04	0.02	0.4	77.5	17.2	15.0	23.0	1.54	0.22	48.3	15.0	0.08	16.2
DB11-35	Harzburgite	3.244	1,817	56.0	0.07	0.05	0.7	62.4	17.7	26.5	44.2	1.67	0.28	31.5	11.2	0.07	7.1
DB11-39	Harzburgite	3.147	5,605	178.1	0.22	0.55	2.5	92.7	19.3	16.1	25.3	1.57	0.21	10.8	7.6	0.10	19.4
DB11-40	Harzburgite	3.199	1,081	33.8	0.04	0.02	0.5	26.5	9.32	28.7	46.0	1.60	0.35	27.6	12.6	0.03	12.9
DB11-41	Harzburgite	3.081	4,563	148.1	0.18	0.06	0.4	141.4	41.3	22.9	37.3	1.63	0.29	27.9	12.4	0.15	28.0
DB11-43	Harzburgite	3.108	15,400	495.4	0.60	5.85	9.7	539.7	99.5	13.1	21.6	1.65	0.18	20.1	10.4	0.59	24.4
DB11-44	Harzburgite	3.082	12,806	415.5	0.50	1.98	4.0	474.5	76.0	12.9	23.7	1.84	0.16	18.3	11.8	0.52	27.8
DB11-46	Harzburgite	3.048	2,153	70.6	0.08	0.02	0.3	124.2	19.9	14.8	32.3	2.18	0.16	28.3	12.2	0.14	32.1
DB11-48	Harzburgite	3.275	1,441	44.0	0.06	0.02	0.4	70.9	11.0	19.4	42.7	2.20	0.16	25.1	10.7	0.08	3.2
DB11-49	Harzburgite	3.242	1,339	41.3	0.05	0.14	2.7	18.0	2.41	18.0	49.1	2.73	0.13	5.84	15.1	0.02	7.4
DB11-50	Harzburgite	3.236	1,128	34.9	0.04	0.09	1.9	24.3	4.81	18.3	37.6	2.06	0.20	13.8	11.5	0.03	8.2
DB11-51	Harzburgite	3.317	890	26.8	0.03	0.02	0.5	11.0	2.53	24.7	48.6	1.97	0.23	9.42	10.4	0.01	0.0
DB11-52	Harzburgite	3.245	974	30.0	0.04	0.90	23.7	33.0	6.30	18.8	41.2	2.20	0.19	21.0	16.2	0.04	7.0
DB11-53	Harzburgite	3.302	898	27.2	0.04	0.01	0.3	16.3	3.65	22.5	44.3	1.97	0.22	13.4	10.4	0.02	0.0
DB11-29	Serpentinite	2.618	48,070	1836	1.87	0.95	0.5	1671	326.5	16.6	29.6	1.78	0.20	17.8	2.9	1.82	86.9
Mean[b]		3.152	2,202	70.3	0.09	0.42	6.4	70.6	14.0	20.1	38.8	1.94	0.22	19.6	12.7	0.08	19.0

[a] ρ, density; κ, volume susceptibility; χ, mass susceptibility; J_i, induced magnetization; NRM, natural remanent magnetization; Q_n, Köenigsberger ratio (= NRM/J_i, SI). M_s, saturation magnetization; M_{rs}, saturation remanence; B_c, coercivity; B_{cr}, coercivity of remanence; χ_{para}, paramagnetic susceptibility; m, the content of magnetite; S, the degree of serpentinization.

[b] The mean of $S < 60\%$ serpentinized samples excluding DB11-29.

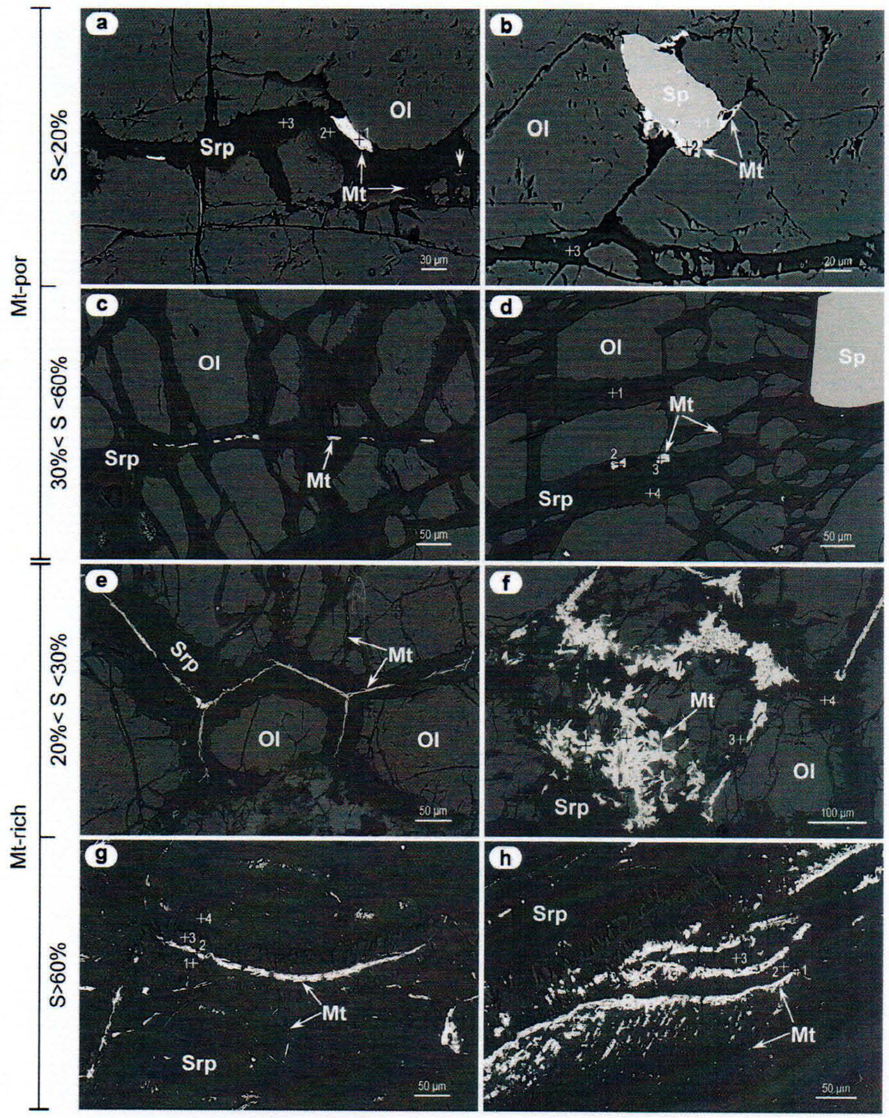

Figure 2. BSE images of variably serpentinized peridotites from the Dongbo ophiolite. (a, b) DB11-52, harzburgite (*S*~7%). a-1, Mt; a-2 and a-3, Srp. b-1, Sp; b-2, Mt; and b-3, Srp. (c, d) DB11-58, dunite (*S*~51%). d-1 and d-4, Srp; d-2 and d-3, Mt. (e, f) DB11-43, harzburgite (*S*~24%). f-1 and f-2, Mt; f-3 and f-4, Fe-poor Srp. (g, h) DB11-29, harzburgite (*S*~87%). g-1 and g-3, Fe-poor Srp; g-2, Mt; g-4, Srp. h-1, Mt; h-2 and h-3, Fe-poor Srp. The cross indicates the analysis spot (Tables 2 and 3). *S*, the degree of serpentinization. Ol, olivine; Sp, spinel; Srp, serpentine; and Mt, magnetite.

(field cooling, FC) and warmed back to 300 K in zero field. Samples were then cooled again to 20 K in zero-field (zero-field cooling, ZFC) and imparted a low-temperature saturation isothermal remanent magnetization (LTSIRM) in 2.5 T field at 20 K. FC followed by ZFC remanence curves were measured on warming in zero field to 300 K in 5 K increments. Samples were then given a 2.5 T SIRM at 300 K (RTSIRM), and magnetization was measured during cooling to 20 K and warming back to 300 K in zero field at 5 K increments. The residual field for zero-field measurements in the MPMS-5S susceptometer is less than 1 μT after adjustment using the susceptometer's ultralow field option.

3.2. Petrographic and Mineral Chemical Analyses

The degree of serpentinization (*S*) was estimated from the empirical relationship between *S* and density for ultramafic rocks as ρ (g cm^{-3}) = 3.300 0.785 × *S* [*Miller and Christensen*, 1997]. Backscattered electron (BSE)

Table 2. Electron Microprobe Analyses of Silicates for the Dongbo Peridotites

Sample	Mineral	Spot[a]	SiO_2	TiO_2	Al_2O_3	Cr_2O_3	FeO_{total}	MnO	MgO	CaO	Na_2O	K_2O	NiO	Total	X_{Mg}[b]
DB11-52	Ol		40.69	0.01	0.00	0.03	8.88	0.12	49.00	0.03	0.00	b.d.	0.31	99.07	
	Srp	a-2	42.38	b.d.	0.04	b.d.	7.43	0.10	32.50	0.32	b.d.	0.00	0.04	82.80	0.89
	Srp	a-3	41.40	0.01	0.05	0.04	6.67	0.13	35.90	0.08	0.02	0.01	0.18	84.48	0.91
	Srp	b-3	41.77	0.02	0.21	0.05	7.04	0.06	32.98	0.16	b.d.	0.00	0.40	82.68	0.89
DB11-58	Ol		41.04	b.d.	b.d.	0.08	8.39	0.09	49.40	0.01	b.d.	0.00	0.43	99.44	
	Srp	d-1	36.81	b.d.	0.00	0.01	5.30	0.03	38.06	0.03	0.01	0.01	0.12	80.38	0.93
	Srp	d-4	34.43	0.00	0.02	b.d.	6.22	0.02	40.31	0.01	0.05	0.01	0.29	81.34	0.92
DB11-43	Ol		41.06	0.02	0.01	0.01	9.35	0.12	48.95	0.04	0.02	b.d.	0.33	99.89	
	Fe-poor Srp	f-3	42.64	0.03	0.05	0.03	2.20	0.08	39.39	0.03	0.01	0.00	0.09	84.55	0.97
	Fe-poor Srp	f-4	43.56	b.d.	0.83	b.d.	3.67	0.04	37.60	b.d.	0.01	b.d.	0.24	85.94	0.95
	Fe-poor Srp		44.04	0.03	0.16	b.d.	3.36	0.07	38.11	b.d.	b.d.	0.01	0.16	85.94	0.95
	Fe-poor Srp		43.28	0.02	0.94	0.01	3.99	0.04	37.10	b.d.	0.01	b.d.	0.14	85.52	0.94
DB11-29	Fe-poor Srp	g-1	44.06	0.02	0.05	b.d.	3.57	b.d.	38.54	0.02	b.d.	b.d.	0.32	86.58	0.95
	Fe-poor Srp	g-3	43.66	0.01	0.14	b.d.	3.40	0.10	38.66	0.01	0.01	0.00	0.26	86.24	0.95
	Srp	g-4	40.47	b.d.	0.27	0.04	5.23	0.14	36.31	0.07	b.d.	b.d.	0.27	82.80	0.93
	Fe-poor Srp	h-2	42.75	0.02	0.16	b.d.	2.40	b.d.	40.69	0.03	0.00	b.d.	0.17	86.22	0.97
	Fe-poor Srp	h-3	42.61	0.02	0.23	b.d.	2.97	0.03	40.05	0.04	0.01	b.d.	0.27	86.23	0.96

[a]The spots refer to Figure 2.
[b]X_{Mg} = Mg/(Mg+ΣFe). b.d., below detection.

images and element mapping of representative occurrences of magnetic minerals were collected on polished thin sections (~0.1 mm thick) using a field emission scanning electronic microscope (Zeiss Sigma 300), equipped with energy dispersive spectroscopy detectors (Oxford Instruments) at CUG (Wuhan), with a working distance of 8.5 mm and an accelerating voltage of 20 kV. The quantitative chemical compositions of iron-oxides and serpentine minerals were analyzed using a Jeol JXA-8100 electron probe microanalyzer, with a spot size of 1–5 μm at 15 kV, at the State Oceanic Administration of China (Hangzhou).

4. Results

4.1. Petrography

The Dongbo peridotites in this study consist of five dunite samples and 28 harzburgite samples, and show a range of densities from 3.317 to 2.618 g cm^{-3}, corresponding to slight to intermediate serpentinization degrees ($S < 60\%$) except for one highly serpentinized sample (DB11-29, S~87%) (Table 1). Samples with

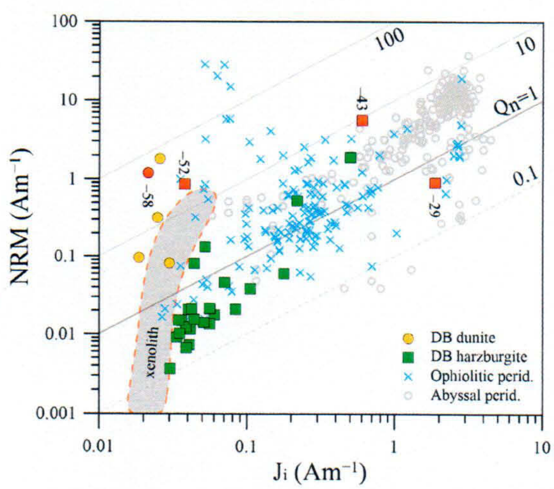

Figure 3. Plot of induced magnetization (J_i) versus natural remanent magnetization (NRM) for variably serpentinized peridotites. Peridotite xenoliths from *Li et al.* [2015] and *Ferré et al.* [2013], abyssal peridotites from *Oufi et al.* [2002], and ophiolitic peridotites from *Maffione et al.* [2014].

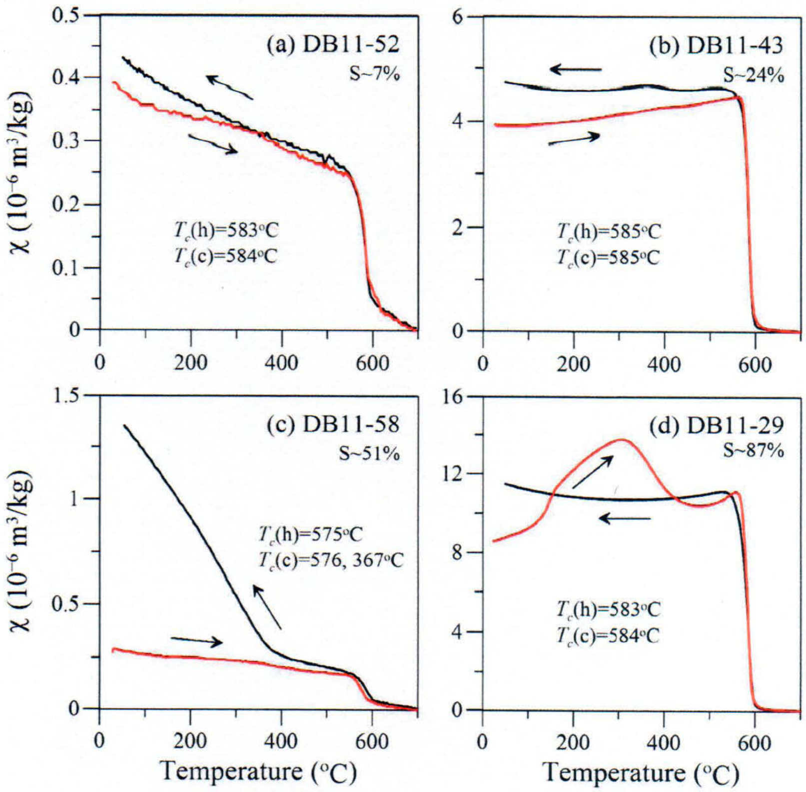

Figure 4. χ-T curves of representative Dongbo peridotites. The arrows indicate the heating (red) and cooling (black) curves. The Curie temperatures of $T_c(h)$ and $T_c(c)$ are estimated from the minimum curvature of the first derivative of smoothed curves.

$S < 20\%$ or $30\% < S < 60\%$ contain low contents of magnetite (<0.1 wt %), calculated from the ratio of mass-specific saturation magnetization of samples to that of pure magnetite ($M_S = 92$ Am^2 kg^{-1}). In contrast, peridotites in the range of $20\% < S < 30\%$ contain higher amounts of magnetite (up to 0.6 wt %), while the $S > 60\%$ serpentinized sample (DB11-29) is richest in magnetite (~1.82 wt %) (Figure 2).

According to the occurrence and chemical compositions of serpentine minerals (Table 2), at least two generations of serpentine (± brucite) veins have been recognized in the Dongbo peridotites. Type 1 veins are narrow in width (<100 μm) and mainly occur in Mt-poor samples (e.g., DB11-52 and DB11-58). These veins consist of Fe-rich serpentine (FeO_{total} = 5.30–8.88 wt %, Table 2) and little magnetite. Magnetite in these veins is predominantly micron or submicron in size, but individual larger grains (20–30 μm) are also present (Figures 2a–2d). Type 2 veins (0.1 mm to cm scale) define anastomosing foliation of Fe-poor serpentine (FeO_{total} = 2.20–3.99 wt %) with one or more magnetite bands/clusters in the interior of the vein (Figures 2e–2h) and are observed only in magnetite-rich peridotites (e.g., DB11-43 and DB11-29). Brucite in serpentine veins is typified by higher MgO contents (37.1–40.7 wt %) in $S > 10\%$ serpentinized samples (DB11-58, DB11-43, and DB11-29) than in $S < 10\%$ serpentinized peridotite (MgO = 32.5–35.9 wt %, DB11-52). Similar type 1 and type 2 serpentine veins in previous studies have been attributed to representative products of early (generally $S < 60\%$) and late ($S > 60$–70%) stages of the serpentinization process [*Beard et al.*, 2009; *Frost et al.*, 2013].

4.2. Magnetic Susceptibility and Natural Remanent Magnetization

The volume-normalized susceptibility (κ) of the Dongbo serpentinized peridotites varies between 476 and 48,070 × 10^{-6} SI, yielding induced magnetizations (J_{i}, = κ H, where H is the local geomagnetic field intensity, equal to 39 Am^{-1}) from 0.02 to 1.87 Am^{-1} (Table 1). The NRMs range widely from ~0 to 5.85 Am^{-1}. Most of the harzburgite samples show linear relations between J_i and NRM, whereas dunites display dominantly low J_i

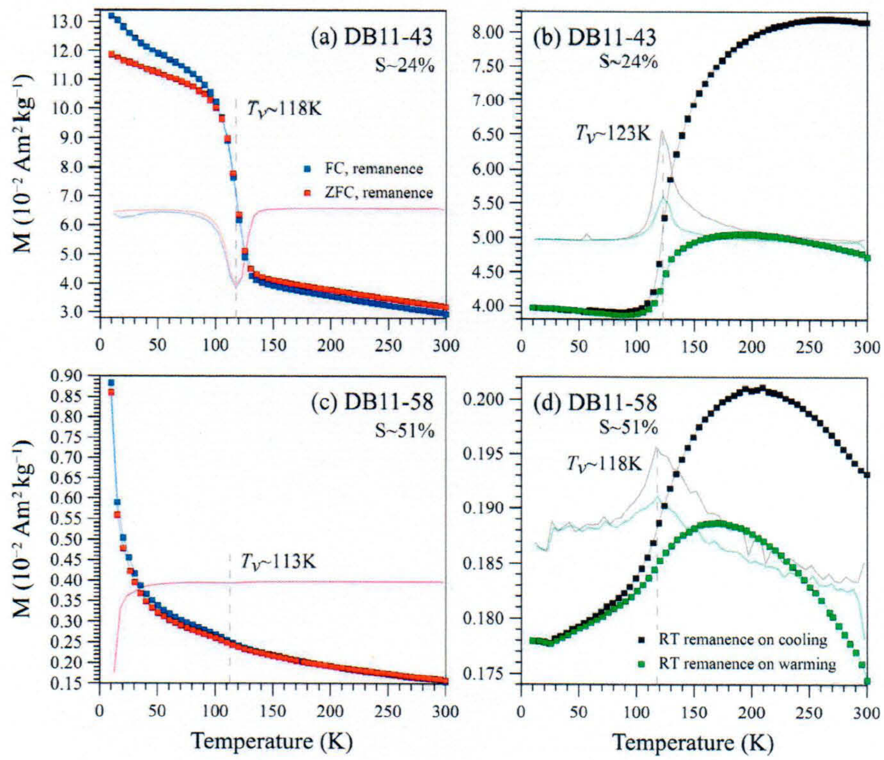

Figure 5. Low-temperature magnetization curves of representative Dongbo peridotites. The Verwey transition (T_V) is estimated from the extreme curvature of the first derivative of smoothed curves.

values. The Köenigsberger ratio (Q_n, defined as NRM/J_i) ranges from 0.13 to 73.4 for all the peridotite samples. Around one third of them display Q_n values greater than 1, which indicates that NRM dominates the total magnetization. The remaining samples show Q_n values less than 1, suggesting that the dominant magnetization is an induced magnetization in the present-day field (Figure 3).

4.3. Thermomagnetic Analyses

High-temperature mass-specific susceptibility (χ-T) were measured for representative samples with different degrees of serpentinization. Sample DB11-52 (S~7%) shows almost reversible heating and cooling curves with Curie temperatures (T_c) of 583–584°C (Figure 4a), which correspond to pure magnetite (T_c 585°C). Samples DB11-43 (S~24%) and DB11-29 (S~87%) also contain pure magnetite with the T_c around 585°C, but the cooling curves are slightly higher than the corresponding heating curves (Figures 4b and 4d). DB1-29 also shows an increase of χ between 150 and 300°C. These features suggest that small amounts of additional magnetite (single T_c at ~585°C on cooling) formed during heating. For sample DB11-58 (S~51%), the Curie temperatures of 575–576°C are slightly lower than the other samples but still indicate magnetite. In addition, the cooling curve of this sample shows a rapid increase below 400°C with a smaller T_c at ~367°C (Figure 4c).

Low-temperature ($T < 300$ K) magnetic experiments were conducted on two representative samples. The FC/ZFC and room temperature (RT) remanence curves show a single Verwey transition (T_V) around 120 K in the harzburgite sample DB11-43 (S~24%) (Figures 5a and 5b), suggesting that magnetite is the dominant remanence-carrying phase. In contrast, for the magnetite-poor dunite sample DB11-58 (S~51%), only a blurred T_V between 110 and 120 K is observed (Figures 5c and 5d), and a hump-shaped warming and cooling RT remanence curves indicate that the magnetite is partially oxidized or mixed with maghemite [*Özdemir and Dunlop*, 2010]. In addition, the FC/ZFC remanence curves for DB11-58 show a rapid decay of magnetization for $T < 50$ K on warming. This decay mimics paramagnetism but the residual during remanence measurements is less than 1 μT making a pure paramagnetic contribution unlikely. A more likely

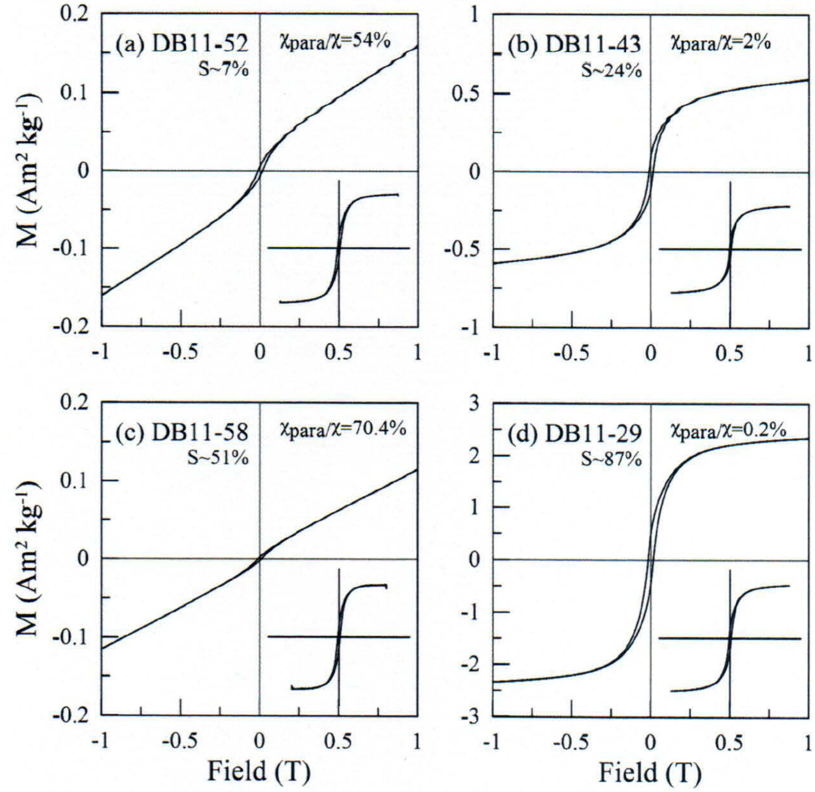

Figure 6. Hysteresis loops of representative Dongbo peridotites. The insets are loops after high-field (0.7-1.0 T) paramagnetic adjustment. The paramagnetic susceptibility (χ_{para}) was from the high-field slope calculation.

explanation (after low-field AC susceptibility as a function of frequency (1–1000 Hz) was measured from 10 to 300 K) is superparamagnetism either from a narrow particle size distribution of ultrasmall grains (e.g., magnetite/maghemite) or a transition from superparamagnetism to paramagnetism of some iron-bearing phase with a magnetic ordering temperature below 50 K (e.g., Fe-Cr spinel).

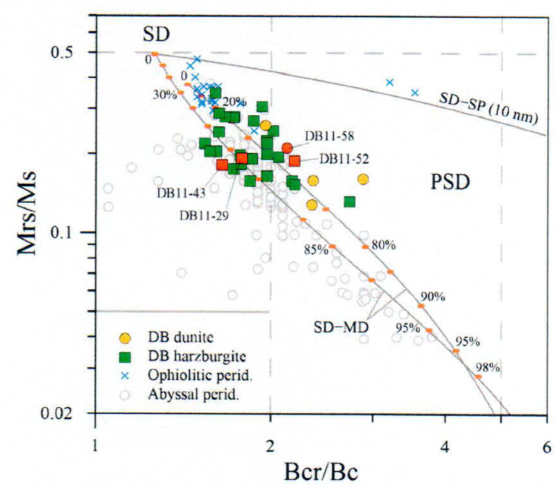

Figure 7. Day plot of various serpentinized peridotites. SD, single domain; PSD, pseudo-single-domain; MD, multidomain; SP, superparamagnetic. The dashed lines and SD-MD/SP (10 nm) mixing curves for magnetite are after *Dunlop* [2002]; the red dots on the SD-MD mixing curves indicate the fractions of MD particles. Abyssal and ophiolitic peridotites are from the references shown in Figure 3.

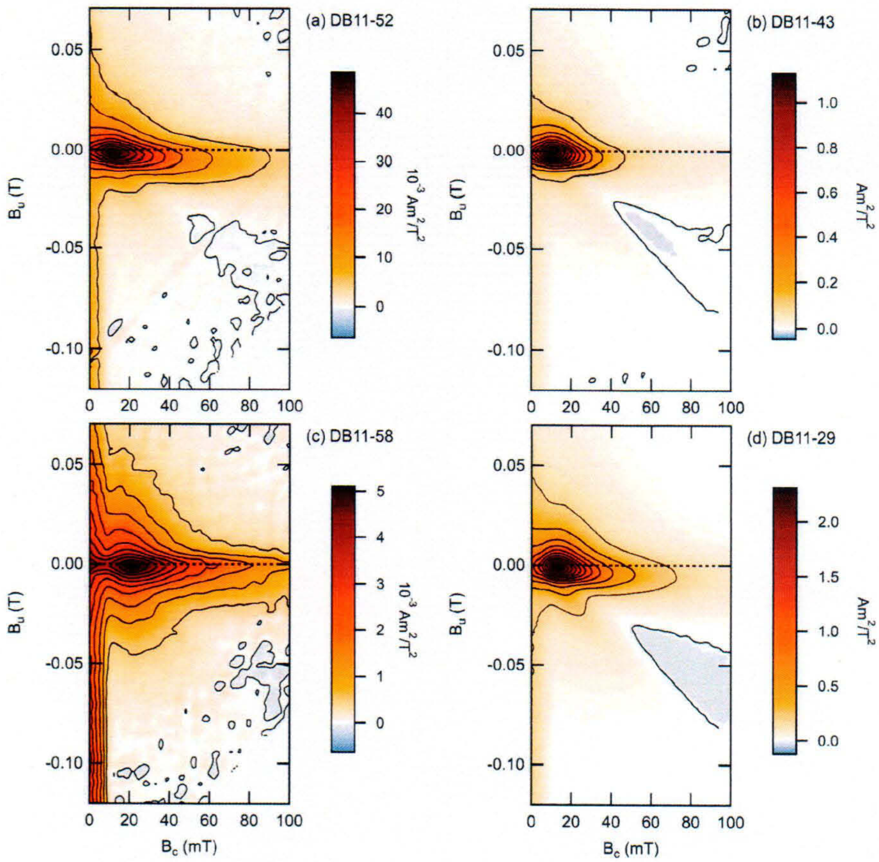

Figure 8. FORC diagrams of representative Dongbo serpentinized peridotites. FORCs were processed using FORCinel 3.0 with drift correction, first/last point replacement, lower branched subtraction (10 FORCs) and a smoothing factor of 5.

4.4. Magnetic Hysteresis

Magnetic hysteresis loops of representative samples are shown in Figure 6. Samples DB11-52 and DB11-58 are weakly magnetic and mainly show linear relationships between the field and the magnetization before paramagnetic correction. Paramagnetic susceptibility (χ_{para}) contributes greater than 50% of the initial susceptibility. Samples DB11-43 and DB11-29 are dominantly ferrimagnetic with χ_{para} contributions less than 5%. These results are consistent with the thermomagnetic analyses. Hysteresis parameters (M_s, M_{rs}, B_c, and B_{cr}) for all the samples are summarized in Table 1. The M_s and M_{rs} values have a wide range from 3.36 to 1671 $\times$ 10^{-3} Am^2 kg^{-1} and from 0.54 to 327 $\times$ 10^{-3} Am^2 kg^{-1}, while B_c and B_{cr} vary between 12.9 and 28.8 mT, and between 21.6 and 59.4 mT, respectively. The Day plot (M_{rs}/M_s versus B_{cr}/B_c) [*Day et al.*, 1977] indicates that the magnetic particles (essentially magnetite from the χ-T results) in the Dongbo serpentinized peridotites mainly fall in the pseudo-single-domain (PSD) region (Figure 7). The hysteresis data mostly follow theoretical trends for mixtures of single domain (SD, <0.1 μm) and multidomain (MD, >1 μm) magnetite. However, some harzburgite (e.g., DB11-52) and dunite samples (e.g., DB11-58) plot above the SD-MD mixing curves but below the SD-SP (10 nm) mixing curve, suggesting minor contributions from superparamagnetic (SP, ≪0.5 μm) particles.

4.5. FORCs

FORCs were measured to further characterize the magnetic grain size distributions (Figure 8). The FORC diagrams of representative peridotite samples display peaks in the FORC distribution between 10 and 20 mT, and spreading about the horizontal B_c axis. These features are commonly associated with interacting SD grains. The divergence of outer contour lines that spread out toward the $B_c = 0$ is more of a property of PSD grains (DB11-43 and DB11-29). The asymmetric vertical FORC distribution along the B_u axis for DB11-29 also indicates the presence of MD grains [*Pike et al.*, 2001; *Roberts et al.*, 2014]. The FORC

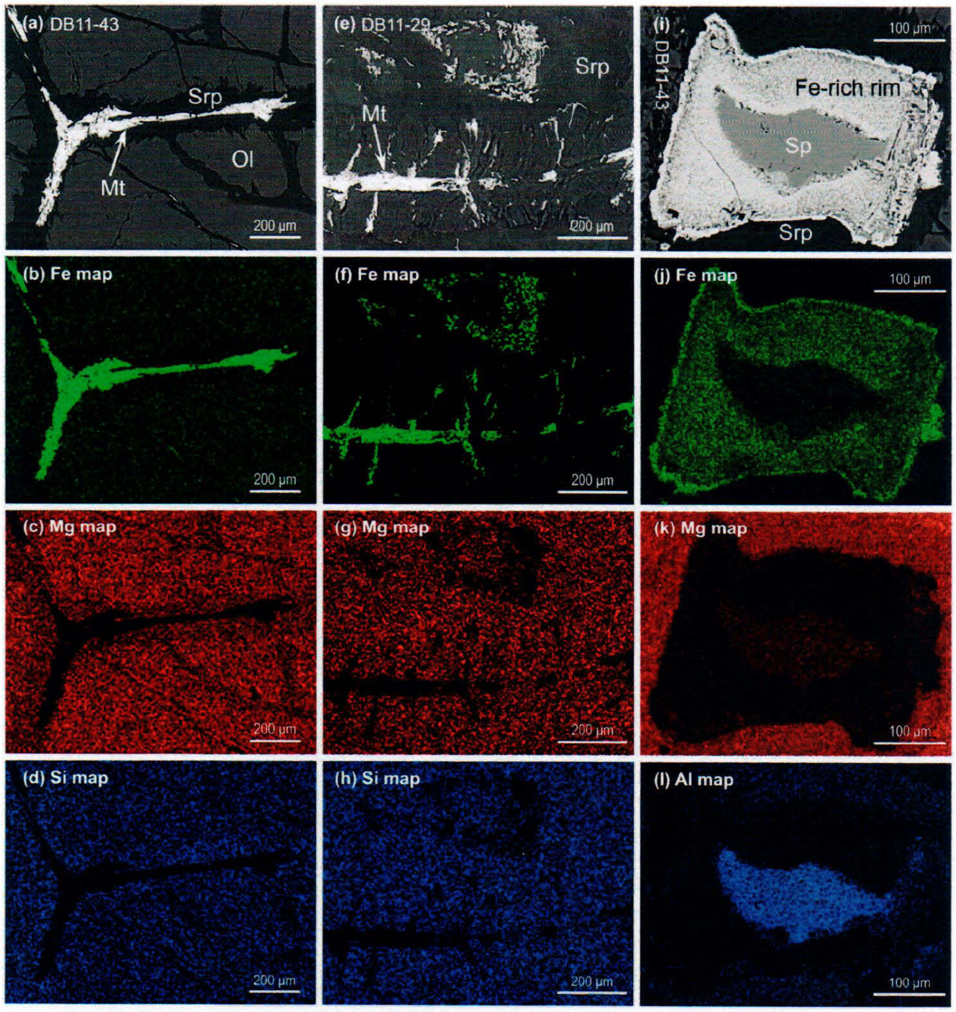

Figure 9. BSE images and element maps of representative magnetite microstructures in the Mt-rich Dongbo peridotites. (a–d) Magnetite bands in the interior of serpentine veins. (e–h) Magnetite structures in the >60% serpentinized peridotites. (i–l) Spinel develops Fe-rich oxidation rims with outermost overgrowth of pure magnetite.

diagrams therefore indicate mixtures of interacting SD magnetite, and PSD and/or MD magnetite in the Dongbo serpentinized peridotites. Furthermore, DB11-58 (and possibly DB11-52) contains an additional component with a smaller distribution peak near the origin and nearly vertical contours extending below the B_c axis, consistent with superparamagnetic grains [*Roberts et al.*, 2014]. Superparamagnetic behavior in DB11-58 was also inferred from the low-temperature FC/ZFC remanence curves as mentioned there (Figure 5c); however, it is unclear if the superparamagnetism detected at $T < 50$ K is carried by a Fe-bearing phase that is magnetically ordered at room temperature.

5. Discussion

5.1. Magnetic Phases in the Dongbo Serpentinized Peridotites

The M_{rs}/χ and B_{cr} values of the Dongbo serpentinized peridotites range from 5.84 to 48.3 × 10^3 Am^{-1} and from 21.6 to 58.1 mT (Table 1), respectively, falling in the magnetite/titanomagnetite region [*Peters and Dekkers*, 2003]. Various magnetites in serpentine veins are the predominant occurrence (Figure 9), and the magnetite grains are nearly pure Fe_3O_4 in chemical composition (Table 3). This is consistent with the high- and low-temperature magnetic analyses (Figures 4 and 5), which reveal that magnetite is the principal magnetic phase controlling the magnetic properties of the Dongbo serpentinized peridotites.

Table 3. Electron Microprobe Analyses of Oxides for the Dongbo Peridotites

Sample	Mineral	Spot[b]	SiO_2	TiO_2	Al_2O_3	FeO_{total}	Cr_2O_3	MnO	MgO	CaO
DB11-52	Mt	a-1	1.63	0.03	0.01	89.61	0.02	0.04	0.88	0.02
	Mg-Al Sp	b-1	b.d.	0.00	37.05	16.58	29.38	0.14	15.32	0.01
	Mt	b-2	0.16	b.d.	0.02	91.26	0.69	0.11	0.51	0.01
DB11-58	Mt	d-2	0.33	0.02	0.02	89.48	0.03	0.77	0.32	0.01
	Mt	d-3	0.71	b.d.	0.01	89.14	b.d.	1.04	0.60	b.d.
	Fe-Cr Sp		0.01	0.09	11.73	24.24	54.86	0.39	8.53	0.01
	Fe-Cr Sp		0.03	0.09	11.65	25.16	53.66	0.44	7.66	0.00
DB11-43	Mt	f-1	0.05	0.00	0.03	91.38	b.d.	b.d.	0.38	0.01
	Mt	f-2	0.06	b.d.	b.d.	93.41	0.06	0.07	0.36	0.01
	Mt		0.05	b.d.	b.d.	92.69	0.08	0.09	0.33	b.d.
	Mg-Al Sp		0.03	0.04	35.10	17.97	31.04	0.21	14.58	0.03
	Sp rim[a]		1.32	0.11	0.79	62.02	28.46	0.78	1.99	0.03
DB11-29	Mt	g-2	0.53	0.00	0.01	91.33	0.01	0.05	0.11	0.00
	Mt	h-1	0.53	0.02	0.02	90.97	b.d.	0.08	0.50	b.d.
	Mt		0.33	0.01	b.d.	91.41	0.35	0.04	0.42	0.00
	Mg-Al Sp		0.02	0.07	39.81	15.71	25.39	0.20	16.58	b.d.

[a]Spinel's oxidation rim.
[b]The spot refers to Figure 2.
[c]The mole fraction of end-members $FeCr_2O_4$ and Fe_3O_4 in spinel.
[d]Mineral formula calculation from *Ghiorso and Sack* [1995].

Spinels in the Dongbo harzburgites are primarily Fe-Cr-rich Mg-Al spinel with 0.25–0.34 mole fractions of $FeCr_2O_4$, assuming that the spinel end-members are $FeCr_2O_4$, $MgCr_2O_4$, $MgAl_2O_4$, and Fe_3O_4 (Table 3). The Mg-Al spinel commonly develops an oxidation rim with outermost overgrowth of pure magnetite. The oxidation rim becomes richer in Fe toward the spinel boundary and becomes wider in DB11-43 (S~24%) (Figure 9) than in DB11-52 (S~7%) (Figure 2b), suggesting increasing oxidation state for magnetite-rich serpentinized peridotites.

In contrast, spinels in the dunites (e.g., DB11-58) are dominantly Fe-Cr spinel with 0.53–0.56 moles of $FeCr_2O_4$ and <0.1 of Fe_3O_4 (Table 3), and the spinels do not show any oxidation rims. Fe_3O_4-poor spinels generally show paramagnetic susceptibility [*Harrison and Putnis*, 1996], and this is supported by the χ-T curve of sample DB11-58 without T_c below 550°C during heating (Figure 4c). The new T_c at ~367°C on cooling could be caused by the formation of new Fe_3O_4-rich spinel and another Fe-poorer spinel during high-temperature heating [*Li et al.*, 2014]. The Fe_3O_4-poor Fe-Cr spinels may also account for the rapid rise of magnetization at $T < 50$ K (Figure 5c) like pure $FeCr_2O_4$ [*Robbins et al.*, 1971]. Though some Fe_3O_4-rich Fe-Cr spinel could carry NRM at $T < 200$°C [*Yu et al.*, 2001], it is unclear whether or not the Fe_3O_4-poor Fe-Cr spinels contribute to the high NRM (>1 Am^{-1}) in the Dongbo dunite samples (Figure 3).

5.2. Magnetic Variations in Variably Serpentinized Peridotites

Various serpentinized peridotites from oceanic and continental regions have shown wide variations in the relationship between magnetic susceptibility and density or the serpentinization degree [*Beard et al.*, 2009]. For the Dongbo peridotites, magnetic susceptibility and the magnetite content exhibit a coupled relationship with increasing serpentinization (Figures 10a and 10b), indicating that magnetite abundance dominantly controls susceptibility. The highly serpentinized sample DB11-29 (S~87%) contains the highest magnetite content of ~1.82 wt %, consistent with other $S > 60\%$ serpentinized abyssal peridotites [*Oufi et al.*, 2002]. However, for the other peridotite samples, magnetite abundance shows an increase from 0.01 to ~0.1 wt % for $S < 20\%$ of serpentinization, and then an apparent decrease from ~0.15 to <0.02 wt % between S~30% and ~60% of serpentinization. A narrow peak of magnetite abundance (up to 0.6 wt %) is at S~25% of serpentinization (ρ, ~3.1 ± 0.05 g cm^{-3}) (Figure 10a). These features are distinctive from the generally positive correlation between the magnetite content and the degree of serpentinization observed in other ophiolitic peridotites [e.g., *Maffione et al.*, 2014].

The decrease in magnetite abundance for the S = 30–60% serpentinized Dongbo peridotites is mainly observed in dunite samples (Figure 10a). These samples display low susceptibilities (<1.0 × 10^{-3} SI,

Table 3. (continued)

Sample	Na_2O	K_2O	NiO	Total	$X_{FeCr2O4}$ [c]	X_{Fe3O4} [c]	Referential Formula [d]
DB11-52	0.02	0.01	0.09	92.36			$(Mg_{0.05}Fe^{2+}_{0.95}Fe^{3+}_{2})_3O_4$
	b.d.	b.d.	b.d.	98.48	0.31	0.03	$(Fe^{2+}_{0.34}Mg_{0.66})(Fe^{3+}_{0.06}Al_{1.26}Cr_{0.67})_2O_4$
	b.d.	0.01	1.05	93.82			$(Mg_{0.03}Fe^{2+}_{0.97}Fe^{3+}_{1.98}Cr_{0.02})_3O_4$
DB11-58	0.01	b.d.	0.14	91.14			$(Mg_{0.02}Fe^{2+}_{0.98}Fe^{3+}_{2})_3O_4$
	0.05	0.01	0.23	91.79			$(Mg_{0.04}Fe^{2+}_{0.96}Fe^{3+}_{2})_3O_4$
	b.d.	0.01	0.07	99.94	0.53	0.05	$(Fe^{2+}_{0.58}Mg_{0.42})(Fe^{3+}_{0.09}Al_{0.46}Cr_{1.44})_2O_4$
	b.d.	b.d.	0.09	98.79	0.56	0.06	$(Fe^{2+}_{0.62}Mg_{0.39})(Fe^{3+}_{0.10}Al_{0.46}Cr_{1.44})_2O_4$
DB11-43	b.d.	b.d.	0.29	92.15			$(Mg_{0.02}Fe^{2+}_{0.98}Fe^{3+}_{2})_3O_4$
	0.03	b.d.	0.23	94.23			$(Mg_{0.02}Fe^{2+}_{0.98}Fe^{3+}_{2})_3O_4$
	0.00	b.d.	0.36	93.62			$(Mg_{0.02}Fe^{2+}_{0.98}Fe^{3+}_{2})_3O_4$
	0.01	0.00	0.16	99.17	0.34	0.03	$(Fe^{2+}_{0.37}Mg_{0.63})(Fe^{3+}_{0.07}Al_{1.21}Cr_{0.72})_2O_4$
	0.03	0.01	0.09	95.61	0.41	0.48	$(Fe^{2+}_{0.89}Mg_{0.11})(Fe^{3+}_{1.10}Al_{0.04}Cr_{0.86})_2O_4$
DB11-29	b.d.	b.d.	0.08	92.12			$(Mg_{0.01}Fe^{2+}_{0.99}Fe^{3+}_{2})_3O_4$
	b.d.	b.d.	0.03	92.15			$(Mg_{0.03}Fe^{2+}_{0.97}Fe^{3+}_{2})_3O_4$
	0.00	0.00	0.44	93.01			$(Mg_{0.02}Fe^{2+}_{0.98}Fe^{3+}_{1.99}Cr_{0.01})_3O_4$
	0.02	b.d.	0.30	98.08	0.25	0.04	$(Fe^{2+}_{0.29}Mg_{0.71})(Fe^{3+}_{0.08}Al_{1.34}Cr_{0.57})_2O_4$

Figure 10b) like the freshest harzburgites and minor dunite samples from the Dun Mountain ophiolite in New Zealand [*Hatherton*, 1967], which plot below the dominantly negative density-susceptibility line/zone for other peridotite samples [*Frost and Beard*, 2007; *Oufi et al.*, 2002]. Generally, the serpentinization of peridotite is a fluid-involved reaction sequence with serpentine, brucite, and magnetite forming primarily from the breakdown of olivine and/or pyroxene with peak formation of magnetite at >60–70% of the serpentinization [*Bach et al.*, 2006; *Toft et al.*, 1990]. The serpentine (± brucite) veins in magnetite-poor dunite (DB11-58) and harzburgite (DB11-52) samples contain low SiO_2 contents of 34.4–42.4 wt % and low X_{Mg} (Mg/(Mg+ΣFe)) of 0.89–0.93 (Table 2). These results follow the evolution trend for Fe-rich serpentine-brucite minerals reported by *Klein et al.* [2014], who documented that temperatures <~200°C lead to Fe-rich brucite and relatively little magnetite in serpentinized mantle peridotites.

The Dongbo dunites probably have experienced dominantly low-temperature (<~200°C) serpentinization by reactions of olivine to Fe-rich serpentine-brucite minerals with the formation of rare magnetite [*Klein et al.*, 2014; *Seyfried et al.*, 2007] before *S*~60–70% of serpentinization. Moreover, external input of SiO_2(aq) from either the reaction of orthopyroxene [*Klein et al.*, 2009] or modified seawater [*Alt and Shanks*, 2003] will result in high silica activities in the serpentinization systems and facilitate the formation of magnetite. However, within the dunite lenses (a relatively closed system), silica is limited due to either lack of orthopyroxene or direct infiltration of large amounts of external silica-rich fluids, which suppresses the extraction of magnetite from Fe-rich serpentine-brucite minerals even at higher degrees of serpentinization (e.g., S = 30–60%). Therefore, the low magnetite abundance in the S = 30–60% serpentinized Dongbo dunites, as well as minor harzburgite samples, should not refer to a reduction or consumption of magnetite from the peak abundance at *S*~25% for harzburgites but probably resulted from combined low-temperature and low-silica activity serpentinization within the Dongbo ophiolite.

In contrast, the Fe-poor serpentine-brucite veins in magnetite-rich harzburgite samples (DB11-43 and DB11-29) show comparatively higher X_{Mg} of 0.94–0.97, suggesting serpentinization temperatures of 200–400°C [*Andreani et al.*, 2013; *Klein et al.*, 2014]. Moreover, the Fe-poor serpentine veins generally form in fluid-dominated systems [*Beard et al.*, 2009; *Frost et al.*, 2013], where the infiltration of oxidizing fluids drives the reactions of Fe-rich serpentine and brucite to magnetite. Therefore, the narrow peak of magnetite abundance at *S*~25% of serpentinization for the Dongbo harzburgite samples (Figure 10a) may indicate localized short-term injection of fluids at ~200–400°C, similar to that abundant magnetite is produced in the S > 60–70% serpentinized peridotites with high fluid/rock ratios in open systems [e.g., *Bach et al.*, 2006; *Beard et al.*, 2009].

Magnetic domain structures in magnetite also show variations in the serpentinization process [e.g., *Fujii et al.*, 2017; *Maffione et al.*, 2014]. Fine-grained magnetite generally forms during early-stage serpentinization (S < 60%), while coarse grains are products in the S > 60–70% stages [*Bina and Henry*, 1990]. The decrease of M_{rs}/M_s with increasing serpentinization degree for the Dongbo serpentinized peridotites is

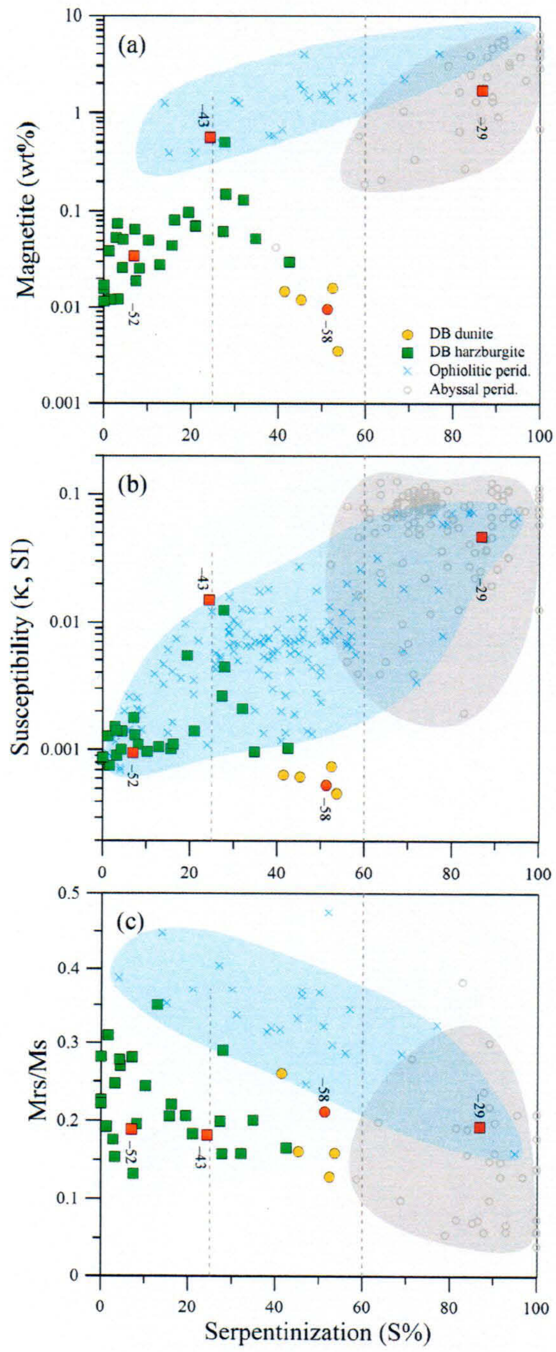

Figure 10. Magnetic variations with increasing degrees of serpentinization for various peridotites. Abyssal peridotites in gray and ophiolitic peridotites in blue (references shown in Figure 3).

broadly consistent with this suggestion (Figure 10c). However, the low-temperature remanence curves (Figure 5) and the FORC diagrams (Figure 8) suggest a small but weakly defined contribution from ultrafine-grained SP particles (possibly magnetite) may form in intermediately serpentinized (S = 10–60%) but magnetite-poor dunites (e.g., DB11-58), in addition to their occurrence in slightly serpentinized ($S < 10\%$) peridotites observed elsewhere [e.g., *Maffione et al.*, 2014]. The FORC diagrams and the Day plot (Figure 7) of the Dongbo serpentinized peridotites also suggest that MD magnetite forms in all stages of serpentinization [*Malvoisin et al.*, 2012].

5.3. Origin of Magnetic Anomalies in Suture Zones

Abyssal peridotites have usually experienced high degrees of serpentinization ($S > 60$–70%) with high magnetization intensities of several to tens of Am^{-1} making them significant sources of oceanic magnetic anomalies [*Nazarova*, 1994; *Oufi et al.*, 2002]. However, peridotites with $S < 60\%$ from the Mirdita ophiolite of Albania have an average magnetization intensity of <1 Am^{-1}, which is too low to contribute to oceanic magnetic anomalies [*Maffione et al.*, 2014]; whereas garnet-bearing peridotites in S = 20–60% of serpentinization from the Sulu ultrahigh-pressure orogenic belt in central China have shown much higher NRMs (tens of Am^{-1}) [*Liu et al.*, 2010].

Strong positive aeromagnetic anomalies have been detected in the exposed Dongbo ophiolite area, and an intact magnetic body extending downward ~3–5 km is extrapolated [*Jiang et al.*, 2015, 2016]. Around 70% of the harzburgite samples in this study are weakly magnetic and show J_i and NRM intensities of <0.1 Am^{-1} (Figure 3). Minor dunite and harzburgite samples show high NRMs of ~1 Am^{-1} and also low J_i values of <0.1 Am^{-1}. The highest magnetization intensities lie in the $S > 60\%$ (e.g., DB11-29) and the S = 20–30% serpentinized harzburgite samples (e.g., DB11-43) with >1 Am^{-1} of induced magnetization and up to 5.85 Am^{-1} of the NRM intensities. These samples contain abundant magnetite with high proportions of SD grains (Figures 8 and 9), making them highly susceptible and capable of retaining strong remanences. Therefore, the $S > 60\%$ and $S = 20–30\%$ serpentinized peridotites represent the most magnetic rocks in the Dongbo ophiolite, and peridotites with such degrees of serpentinization are most likely the sources of the large-scale magnetic anomalies [e.g., *Jiang et al.*, 2016] within the Yarlung-Zangbo suture zone in south Tibet.

6. Conclusions

Integrated magnetic, petrographic, and mineral chemical studies of variably serpentinized peridotites from the Dongbo ophiolite in SW Tibet (China) reveal that magnetite is the dominant magnetic phase in all stages of serpentinization. Magnetite typically occurs in serpentine veins but also appears as overgrowth rims of oxidized Mg-Al spinel. The magnetite abundance and magnetic susceptibility show coupled variations with narrow peaks at S~25% of serpentinization (density, ~3.1 ± 0.05 g cm^{-3}). This may suggest a short-term infiltration of fluids and subsequent cutoff of the fluid sources during the serpentinization of the Dongbo peridotites. Dunites in the $S = 30–60\%$ of serpentinization contain Fe-rich serpentine and show very low magnetite abundance, probably resulting from low-temperature and silica-poor serpentinization. Overall, the $S > 60\%$ together with the $S = 20–30\%$ serpentinized peridotites represent the most magnetic rocks in the Dongbo ophiolite, and are significant magnetic sources within the Yarlung-Zangbo suture zone in south Tibet.

Acknowledgments
This work was supported by the China Postdoctoral Science Foundation (2015M572218), the National Science Foundation of China (41504053, 41520104003, and 41374094), and the China Geological Survey (12120115027201). This is IRM contribution 1701. The IRM is supported by the Instruments and Facilities Program of the NSF Division of Earth Science. Mike Jackson and Dario Bilardello from IRM offered generous help in the magnetic measurements. Constructive comments from Mark J. Dekkers (Associate Editor) and two anonymous reviewers have improved the quality of the manuscript. Data presented in this paper can be accessed in the online version at http://dx.doi.org/10.1002/2017JB014241.

References

Alt, J. C., and W. C. Shanks (2003), Serpentinization of abyssal peridotites from the MARK area, Mid-Atlantic Ridge: Sulfur geochemistry and reaction modeling, *Geochim. Cosmochim. Acta*, *67*(4), 641–653, doi:10.1016/S0016-7037(02)01142-0.

Andreani, M., M. Muñoz, C. Marcaillou, and A. Delacour (2013), μXANES study of iron redox state in serpentine during oceanic serpentinization, *Lithos*, *178*, 70–83, doi:10.1016/j.lithos.2013.04.008.

Bach, W., H. Paulick, C. J. Garrido, B. Ildefonse, W. P. Meurer, and S. E. Humphris (2006), Unraveling the sequence of serpentinization reactions: Petrography, mineral chemistry, and petrophysics of serpentinites from MAR 15°N (ODP Leg 209, Site 1274), *Geophys. Res. Lett.*, *33*, L13306, doi:10.1029/2006GL025681.

Beard, J. S., B. R. Frost, P. Fryer, A. McCaig, R. Searle, B. Ildefonse, P. Zinin, and S. K. Sharma (2009), Onset and progression of serpentinization and magnetite formation in olivine-rich troctolite from IODP Hole U1309D, *J. Petrol.*, *50*(3), 387–403, doi:10.1093/petrology/egp004.

Bilardello, D., and M. Jackson (2013), What do the Mumpsies do?, *IRM Q*, *23*, 1–15.

Bina, M. M., and B. Henry (1990), Magnetic properties, opaque mineralogy and magnetic anisotropies of serpentinized peridotites from ODP Hole 670A near the Mid-Atlantic Ridge, *Phys. Earth Planet. Inter.*, *65*(1–2), 88–103, doi:10.1016/0031-9201(90)90078-C.

Blakely, R. J., T. M. Brocher, and R. E. Wells (2005), Subduction-zone magnetic anomalies and implications for hydrated forearc mantle, *Geology*, *33*(6), 445–448, doi:10.1130/G21447.1.

Bonnemains, D., J. Carlut, J. Escartín, C. Mével, M. Andreani, and B. Debret (2016), Magnetic signatures of serpentinization at ophiolite complexes, *Geochem. Geophys. Geosyst.*, *17*, 2969–2986, doi:10.1002/2016GC006321.

Bostock, M. G., R. D. Hyndman, S. Rondenay, and S. M. Peacock (2002), An inverted continental Moho and serpentinization of the forearc mantle, *Nature*, *417*(6888), 536–538, doi:10.1038/417536a.

Dai, J. G., C. S. Wang, R. Hébert, M. Santosh, Y. L. Li, and J. Y. Xu (2011), Petrology and geochemistry of peridotites in the Zhongba ophiolite, Yarlung Zangbo Suture Zone: Implications for the Early Cretaceous intra-oceanic subduction zone within the Neo-Tethys, *Chem. Geol.*, *288*(3–4), 133–148, doi:10.1016/j.chemgeo.2011.07.011.

Day, R., M. Fuller, and V. A. Schmidt (1977), Hysteresis properties of titanomagnetites: Grain-size and compositional dependence, *Phys. Earth Planet. Inter.*, *13*(4), 260–267, doi:10.1016/0031-9201(77)90108-X.

DeCelles, P. G., D. M. Robinson, and G. Zandt (2002), Implications of shortening in the Himalayan fold-thrust belt for uplift of the Tibetan Plateau, *Tectonics*, *21*(6), 1062, doi:10.1029/2001TC001322.

Dunlop, D. J. (2002), Theory and application of the Day plot (M_{rs}/M_s versus H_{cr}/H_c) 1. Theoretical curves and tests using titanomagnetite data, *J. Geophys. Res.*, *107*(B3), 2056, doi:10.1029/2001JB000486.

Evans, B. W., S. M. Kuehner, and A. Chopelas (2009), Magnetite-free, yellow lizardite serpentinization of olivine websterite, Canyon Mountain complex, N.E. Oregon, *Am. Mineral.*, *94*(11–12), 1731–1734, doi:10.2138/am.2009.3301.

Ferré, E. C., S. A. Friedman, F. Martín-Hernández, J. M. Feinberg, J. A. Conder, and D. A. Ionov (2013), The magnetism of mantle xenoliths and potential implications for sub-Moho magnetic sources, *Geophys. Res. Lett.*, *40*, 105–110, doi:10.1029/2012GL054100.

Ferré, E. C., S. A. Friedman, F. Martín-Hernández, J. M. Feinberg, J. L. Till, D. A. Ionov, and J. A. Conder (2014), Eight good reasons why the uppermost mantle could be magnetic, *Tectonophysics*, *624–625*, 3–14, doi:10.1016/j.tecto.2014.01.004.

Frost, B. R., and J. S. Beard (2007), On silica activity and serpentinization, *J. Petrol.*, *48*(7), 1351–1368, doi:10.1093/petrology/egm021.

Frost, B. R., K. A. Evans, S. M. Swapp, J. S. Beard, and F. E. Mothersole (2013), The process of serpentinization in dunite from New Caledonia, *Lithos*, *178*, 24–39, doi:10.1016/j.lithos.2013.02.002.

Fujii, M., K. Okino, H. Sato, K. Nakamura, T. Sato, and T. Yamazaki (2017), Variation in magnetic properties of serpentinized peridotites exposed on the Yokoniwa Rise, Central Indian Ridge: Insights into the role of magnetite in serpentinization, *Geochem. Geophys. Geosyst.*, *17*, 5024–5035, doi:10.1002/2016GC006511.

Ghiorso, M. S., and R. O. Sack (1995), Chemical mass transfer in magmatic processes IV. A revised and internally consistent thermodynamic model for the interpolation and extrapolation of liquid-solid equilibria in magmatic systems at elevated temperatures and pressures, *Contrib. Mineral. Petrol.*, *119*(2–3), 197–212, doi:10.1007/BF00307281.

Harrison, R. J., and J. M. Feinberg (2008), FORCinel: An improved algorithm for calculating first-order reversal curve distributions using locally weighted regression smoothing, *Geochem. Geophys. Geosyst.*, *9*, Q05016, doi:10.1029/2008GC001987.

Harrison, R. J., and A. Putnis (1996), Magnetic properties of the magnetite-spinel solid solution: Curie temperatures, magnetic susceptibilities, and cation ordering, *Am. Mineral.*, *81*(3–4), 375–384.

Hatherton, T. (1967), A geophysical study of Nelson—Cook Strait region, New Zealand, *N. Z. J. Geol. Geophys.*, *10*(6), 1330–1347, doi:10.1080/00288306.1967.10423219.

Jackson, M., and P. Solheid (2010), On the quantitative analysis and evaluation of magnetic hysteresis data, *Geochem. Geophys. Geosyst.*, *11*, Q04Z15, doi:10.1029/2009GC002932.

Jiang, M., J. S. Yang, H. D. Tan, R. Y. Qian, Y. W. Zhang, M. Peng, L. H. Xu, L. S. Zhang, Q. Q. Li, S. Guo, and H. X. Song (2015), Geophysical characteristics and prospecting significance of deep structures in Dongpo ophiolite body, Tibet [in Chinese], *Geol. China*, *42*(5), 1179–1187.

Jiang, M., J. S. Yang, L. S. Zhang, Y. W. Zhang, M. Peng, and Q. Q. Li (2016), The magnetic anomaly characteristics of Dongpo, Xigaze and some other ophiolite rock masses along the Yarlung–Zangbo suture zone and their ore-prospecting significance [in Chinese], *Geol. China*, *43*(5), 1666–1678.

Kelemen, P. B., E. Kikawa, and D. J. Miller (2004), *Proceedings of the Ocean Drilling Program, Initial Rep.*, *209*, Ocean Drill. Program, College Station, Tex., doi:10.2973/odp.proc.ir.209.2004.

Klein, F., W. Bach, N. Jöns, T. McCollom, B. Moskowitz, and T. Berquó (2009), Iron partitioning and hydrogen generation during serpentinization of abyssal peridotites from 15°N on the Mid-Atlantic Ridge, *Geochim. Cosmochim. Acta*, *73*(22), 6868–6893, doi:10.1016/j.gca.2009.08.021.

Klein, F., W. Bach, S. E. Humphris, W. Kahl, N. Jöns, B. Moskowitz, and T. S. Berquó (2014), Magnetite in seafloor serpentinite—Some like it hot, *Geology*, *42*(2), 135–138, doi:10.1130/G35068.1.

Lafay, R., G. Montes-Hernandez, E. Janots, R. Chiriac, N. Findling, and F. Toche (2012), Mineral replacement rate of olivine by chrysotile and brucite under high alkaline conditions, *J. Cryst. Growth*, *347*, 62–72, doi:10.1016/j.jcrysgro.2012.02.040.

Li, Z. Y., J. P. Zheng, Q. L. Zeng, Q. S. Liu, and W. L. Griffin (2014), Magnetic mineralogy of pyroxenite xenoliths from Hannuoba basalts, northern North China Craton: Implications for magnetism in the continental lower crust, *J. Geophys. Res. Solid Earth*, *119*, 806–821, doi:10.1002/2013JB010599.

Li, Z. Y., J. P. Zheng, Q. S. Liu, W. L. Griffin, and X. Y. Hu (2015), Magnetically stratified continental lower crust preserved in the North China Craton, *Tectonophysics*, *643*, 73–79, doi:10.1016/j.tecto.2014.12.012.

Liu, F., J. S. Yang, Y. Dilek, Z. Q. Xu, X. Z. Xu, F. H. Liang, S. Y. Chen, and D. Y. Lian (2015), Geochronology and geochemistry of basaltic lavas in the Dongbo and Purang ophiolites of the Yarlung-Zangbo Suture zone: Plume-influenced continental margin-type oceanic lithosphere in southern Tibet, *Gondwana Res.*, *27*(2), 701–718, doi:10.1016/j.gr.2014.08.002.

Liu, Q. S., Q. L. Zeng, J. P. Zheng, T. Yang, N. Qiu, Z. F. Liu, Y. H. Luo, and Z. M. Jin (2010), Magnetic properties of serpentinized garnet peridotites from the CCSD main hole in the Sulu ultrahigh-pressure metamorphic belt, eastern China, *J. Geophys. Res.*, *115*, B06104, doi:10.1029/2009JB000814.

Liu, Q. S., N. Qiu, J. P. Zheng, Z. Y. Li, and H. C. Wang (2015), Crustal large-scale serpentinized mantle peridotite body in the Sulu ultrahigh-pressure metamorphic belt, eastern China: Evidence from gravity and magnetic anomalies, *J. Struct. Geol.*, *70*, 190–199, doi:10.1016/j.jsg.2014.11.009.

Maffione, M., A. Morris, O. Plümper, and D. J. J. van Hinsbergen (2014), Magnetic properties of variably serpentinized peridotites and their implication for the evolution of oceanic core complexes, *Geochem. Geophys. Geosyst.*, *15*, 923–944, doi:10.1002/2013GC004993.

Malvoisin, B., J. Carlut, and F. Brunet (2012), Serpentinization of oceanic peridotites: 1. A high-sensitivity method to monitor magnetite production in hydrothermal experiments, *J. Geophys. Res.*, *117*, B01104, doi:10.1029/2011JB008612.

Miller, D. J., and N. I. Christensen (1997), Seismic velocities of lower crustal and upper mantle rocks from the slow-spreading Mid-Atlantic Ridge, south of the Kane Transform Zone (MARK), in *Proceedings of the Ocean Drilling Program, Scientific Results*, vol. 153, edited by J. A. Karson, et al., pp. 437–454, College Station, Tex.

Nazarova, K. A. (1994), Serpentinized peridotites as a possible source for oceanic magnetic anomalies, *Mar. Geophys. Res.*, *16*(6), 455–462, doi:10.1007/BF01270519.

Niu, X. L., J. S. Yang, Y. Dilek, J. F. Xu, J. Li, S. Y. Chen, G. Y. Feng, F. Liu, F. H. Xiong, and Z. Liu (2015), Petrological and Os isotopic constraints on the origin of the Dongbo peridotite massif, Yarlung Zangbo Suture Zone, Western Tibet, *J. Asian Earth Sci.*, *110*, 72–84, doi:10.1016/j.jseaes.2014.09.036.

Oufi, O., M. Cannat, and H. Horen (2002), Magnetic properties of variably serpentinized abyssal peridotites, *J. Geophys. Res.*, *107*(B5), 2095, doi:10.1029/2001JB000549.

Özdemir, Ö., and D. J. Dunlop (2010), Hallmarks of maghemitization in low-temperature remanence cycling of partially oxidized magnetite nanoparticles, *J. Geophys. Res.*, *115*, B02101, doi:10.1029/2009JB006756.

Peters, C., and M. J. Dekkers (2003), Selected room temperature magnetic parameters as a function of mineralogy, concentration and grain size, *Phys. Chem. Earth*, *28*(16-19), 659–667, doi:10.1016/S1474-7065(03)00120-7.

Pike, C. R., A. P. Roberts, M. J. Dekkers, and K. L. Verosub (2001), An investigation of multi-domain hysteresis mechanisms using FORC diagrams, *Phys. Earth Planet. Inter.*, *126*(1–2), 11–25, doi:10.1016/S0031-9201(01)00241-2.

Robbins, M., G. K. Wertheim, R. C. Sherwood, and D. N. E. Buchanan (1971), Magnetic properties and site distributions in the system $FeCr_2O_4$-$Fe_3O_4(Fe^{2+}Cr_{2-x}Fe_x^{3+}O_4)$, *J. Phys. Chem. Solids*, *32*(3), 717–729, doi:10.1016/S0022-3697(71)80412-2.

Roberts, A. P., D. Heslop, X. Zhao, and C. R. Pike (2014), Understanding fine magnetic particle systems through use of first-order reversal curve diagrams, *Rev. Geophys.*, *52*, 557–602, doi:10.1002/2014RG000462.

Seyfried, W. E., D. I. Foustoukos, and Q. Fu (2007), Redox evolution and mass transfer during serpentinization: An experimental and theoretical study at 200°C, 500 bar with implications for ultramafic-hosted hydrothermal systems at Mid-Ocean Ridges, *Geochim. Cosmochim. Acta*, *71*(15), 3872–3886, doi:10.1016/j.gca.2007.05.015.

Toft, P. B., J. Arkani-Hamed, and S. E. Haggerty (1990), The effects of serpentinization on density and magnetic susceptibility: A petrophysical model, *Phys. Earth Planet. Inter.*, *65*(1–2), 137–157, doi:10.1016/0031-9201(90)90082-9.

Wasilewski, P. J., and M. A. Mayhew (1992), The Moho as a magnetic boundary revisited, *Geophys. Res. Lett.*, *19*(22), 2259–2262, doi:10.1029/92GL01997.

Wu, F. Y., C. Z. Liu, L. L. Zhang, C. Zhang, J. G. Wang, W. Q. Ji, and X. C. Liu (2014), Yarlung Zangbo ophiolite: A critical updated view [in Chinese], *Acta Petrol. Sin.*, *30*(2), 293–325.

Xiong, F. H., J. S. Yang, F. H. Liang, D. Z. Ba, J. Zhang, X. Z. Xu, Y. Li, and Z. Liu (2011), Zircon U-Pb ages of the Dongbo ophiolite in the western Yarlung Zangbo suture zone and their geological significance [in Chinese], *Acta Petrol. Sin.*, *27*(11), 3223–3238.

Xiong, Q., W. L. Griffin, J. P. Zheng, S. Y. O'Reilly, N. J. Pearson, B. Xu, and E. A. Belousova (2016), Southward trench migration at ~130–120 Ma caused accretion of the Neo-Tethyan forearc lithosphere in Tibetan ophiolites, *Earth Planet. Sci. Lett.*, *438*, 57–65, doi:10.1016/j.epsl.2016.01.014.

Xu, X. Z., J. S. Yang, D. Z. Ba, Z. M. Zhang, F. H. Xiong, and Y. Li (2015), Diamond discovered from the Dongbo mantle peridotite in the Yarlung Zangbo suture zone, Tibet [in Chinese], *Geol. China*, *42*(5), 1471–1482.

Yang, J. S., F. H. Xiong, G. L. Guo, F. Liu, F. H. Liang, S. Y. Chen, Z. L. Li, and L. W. Zhang (2011), The Dongbo ultramafic massif: A mantle peridotite in the western part of the Yarlung Zangbo suture zone, Tibet, with excellent prospects for a major chromite deposit [in Chinese], *Acta Petrol. Sin.*, *27*(11), 3207–3222.

Yin, A., and T. M. Harrison (2000), Geologic evolution of the Himalayan-Tibetan orogen, *Annu. Rev. Earth Planet. Sci.*, *28*(1), 211–280, doi:10.1146/annurev.earth.28.1.211.

Yu, Y., D. J. Dunlop, Ö. Özdemir, and H. Ueno (2001), Magnetic properties of Kurokami pumices from Mt. Sakurajima, Japan, *Earth Planet. Sci. Lett.*, *192*(3), 439–446, doi:10.1016/S0012-821X(01)00464-2.